Microstructure, strain rate, and temperature effects on the compressive loading behavior of (FeMnNiCo)$_{1-x}$Mo$_x$ high entropy alloy

KRÜGER Lutz[1,a] *, CICHOCKI Kamil[2,b], HENSCHEL Sebastian[1,c],
CHULIST Robert[3,d], BAŁA Piotr[2,e] and MUSZKA Krzysztof[2,f]

[1]TU Bergakademie Freiberg, Institute of Materials Engineering, Gustav-Zeuner-Str. 5, 09599 Freiberg, Germany

[2]AGH University of Science and Technology, Department of Metal Forming and Metallurgical Engineering, al. A. Mickiewicza 30, 30-059 Kraków, Poland

[3]Institute of Metallurgy and Materials Science, Polish Academy of Sciences, ul. W. Reymonta 30, 30-059 Kraków, Poland

[a]krueger@ww.tu-freiberg.de, [b]cichocki@agh.edu.pl, [c]sebastian.henschel@iwt.tu-freiberg.de, [d]r.chulist@imim.pl, [e]pbala@agh.edu.pl [f]muszka@agh.edu.pl

Abstract. High entropy alloys based on FeMnNiCoMo offer a potential for high energy absorption and high strength, even at low temperatures. In this work, the effects of chemical composition and grain size on the mechanical properties were investigated. Compression tests at a wide range of strain rates and temperatures have been performed. For a strain rate of about 10^2 s^{-1} an instrumented drop weight tower was applied. Furthermore, cryogenic temperature tests at -196 °C were carried out. The microstructure was analyzed by means of scanning electron microscopy and transmission Kikuchi diffraction. Hence, the role of grain size, precipitations, and twinning-induced plasticity (TWIP) on the yield strength and the further strain hardening were investigated.

Introduction

High entropy alloys (HEAs) are under focus since the investigations of Cantor et al. [1] and Yeh et al. [2] in 2004. Many alloy systems have been proposed. For some systems, the high ductility and fracture toughness especially at cryogenic temperatures are notable features. A reason for this behavior is the high strain hardening due to solid solution strengthening and deformation twinning [3]. Li et al. [4] suggested dual-phase HEAs which use additional hardening by martensitic phase transformation. A smaller grain size will not only result in a higher strength due to Hall-Petch effect. The stress to induce twinning will also increase [5].

Basu et al. [6] observed a low strain rate sensitivity for the dual-phase Fe$_{50}$Mn$_{30}$Co$_{10}$Cr$_{10}$ alloy at strain rates between 10^{-4} to 5×10^{-3} s^{-1}. Huang et al. [7] reviewed the results of several HEAs at a wide range of strain rates, i.e. 10^{-4} to 10^4 s^{-1}. For the CoCrFeMnNi alloy, an increase in strain rate (10^{-4} to 5×10^3 s^{-1}) leads to a strong increase in strength and work hardening rate. They also investigated the adiabatic heating and determined a rather low Taylor-Quinney coefficient of about 0.5 to 0.6 for strain rates of 10^0 to 3×10^3 s^{-1}. This finding is in contrast to observations of Meyer et al. [8] at a 1045 steel. According to Li et al. [9] the deformation of fcc HEAs at higher strain rates and lower temperatures is mainly based on twinning. This behavior was confirmed in CoCrFeMnNi by Park et al. [10]. However, they did not study the material behavior at intermediate strain rates of about 10^2 s^{-1}. Due to the high work hardening rate, the resistance to adiabatic shear band localization is high [9].

In this work, the mechanical behavior of the system $(FeMnNiCo)_{1-x}Mo_x$ was studied under compressive loading. The effects of Mo content, strain rate and temperature were investigated. In addition to quasi-static and high strain rate tests the mechanical behavior at intermediate strain rates was also measured.

Materials and Methods

Materials. The chemical compositions of the investigated high entropy alloys are given in Table 1. Ingots were produced in a Bühler Arc Melter AM. Further details can be found in a recent study on the phase stability of these alloys [11].

Table 1. Chemical composition of investigated alloys, in atom-%.

Alloy	Fe	Mn	Ni	Co	Mo
FeMnNiCo	24.7	24.2	25.5	25.6	0
$(FeMnNiCo)_{90}Mo_{10}$	22.2	21.2	23.5	23.8	9.3

The ingots were hot rolled at 1100°C with a thickness reduction of 40 %. After air cooling, cold rolling with 6 passes and a total thickness reduction of 10 % was performed. In order to statically recrystallize the microstructure, annealing was done at different temperatures and times. Details are given by Cichocki et al. in this journal issue. The initial microstructure is shown in Fig. 1.
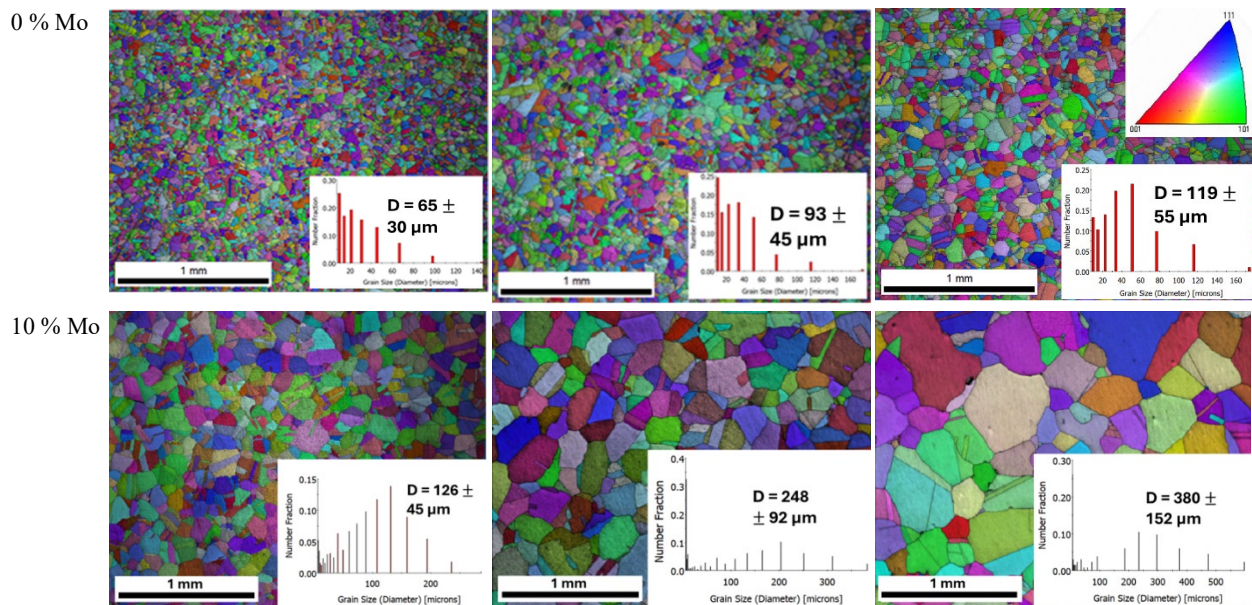

Fig. 1.: Initial microstructure of materials with 0 % Mo (first row) and 10 % Mo (second row).

The different heat treatment led to different average grain sizes and grain size distributions. In all cases, a polygonal grain shape was achieved. Only some annealing twins are visible. The material basically consists of a single phase with fcc lattice. However, it should be noted, that the hard μ phase is present in small amounts in the materials with 10 % Mo [11]. The average grain sizes of the materials are given in Table 2.

Table 2. Average grain sizes and standard deviations of different materials. Grain sizes are referred to by their class name.

Material / Grain size in μm	class A	class B	class C	class D	class E
FeMnNiCo	65 ± 30	93 ± 45	119 ± 55		
$(FeMnNiCo)_{90}Mo_{10}$			126 ± 45	248 ± 92	360 ± 152

To compare the materials, classes of grain sizes were defined. In class C, there are two materials, i.e. 0 % Mo and 10 % Mo. The other classes of grain sizes contain either the 0 % Mo material or the material with 10 % Mo.

Methods. Compression tests were performed at 4 different strain rates: 10^{-1}, 10^0, 10^2 and 10^3 s^{-1}. A bath with liquid nitrogen was applied for the low temperature tests. Tests at strain rates of 10^0 and lower were performed in a universal testing machine. An instrumented drop tower was applied for tests at approximately 10^2 s^{-1}. The drop tower consists of a 190 kg drop weight with a punch that is instrumented with calibrated strain gauges and a 4,000 kg anvil. Strain rates of about 10^3 s^{-1} were achieved in a split Hopkinson pressure bar. The setup consists of incident and transmitted bars, each 2 m long and 20 mm in diameter and made of high-strength maraging steel, which are instrumented with strain gauges. The striker bar had a length of 0.5 m and was made of the same bar material as the other bars. Pulse shaping was used to obtain early force equilibrium and relatively constant strain rates. More details on pulse shaping can be found elsewhere [12]. Interrupted tests at strain rates > 10^{-1} s^{-1} were achieved by stop rings made of high-speed steel with a defined thickness. The samples can only be deformed as long as there is a gap between punch and the stop ring.

In addition to true compressive strain ε and true compressive stress σ, strain hardening coefficient Θ was calculated:

$$\Theta = \frac{d\sigma}{d\varepsilon}. \tag{1}$$

SEM/EBSD analysis of the initial microstructure was performed on a FEI Nova NanoSEM 450 scanning microscope (SEM) using the Velocity EBSD detector from EDAX. The samples were prepared by grinding and mechanical polishing. The EBSD analysis was performed in the center of the compressed sample, with an accelerating voltage of 20 kV and a spot size of 6 with and step size 0.2 μm. HR EBSD was performed in selected samples with a step size of 0.05 μm with an accelerating voltage of 20 kV. Specimens from interrupted compressive tests were analyzed in a Tescan Mira 3 XMU SEM at 15 kV with a Digiview EBSD detector from EDAX and a step size of 0.25 μm. The obtained results were processed with OIM-TSL 8.

Results and Discussion
Effect of Mo content and grain size. The dependence of true stress and strain hardening behavior on the Mo content and the grain sizes is shown in Fig. 2 for room temperature tests at a strain rate of 10^{-1} s^{-1}. It was observed that an increase in Mo results in a higher yield strength, cf. Fig. 2a. This behavior is explained by the solid solution hardening effect. Furthermore, the HEAs with 0 % Mo exhibited a continuously decreasing strain hardening coefficient. The materials with 10 % Mo exhibited a local maximum in strain hardening at a true strain of approximately 0.2.

Within the analyzed range of grain sizes, the materials show an increase in yield strength with decreasing grain size. This is explained by the Hall-Petch effect. However, there is no difference in further strain hardening behavior for the materials with 0 % Mo, cf. Fig. 2b. The material with

10 % Mo and the smallest grain size (class C) exhibited the highest local maximum of the strain hardening coefficient Θ, cf. Fig. 2c.
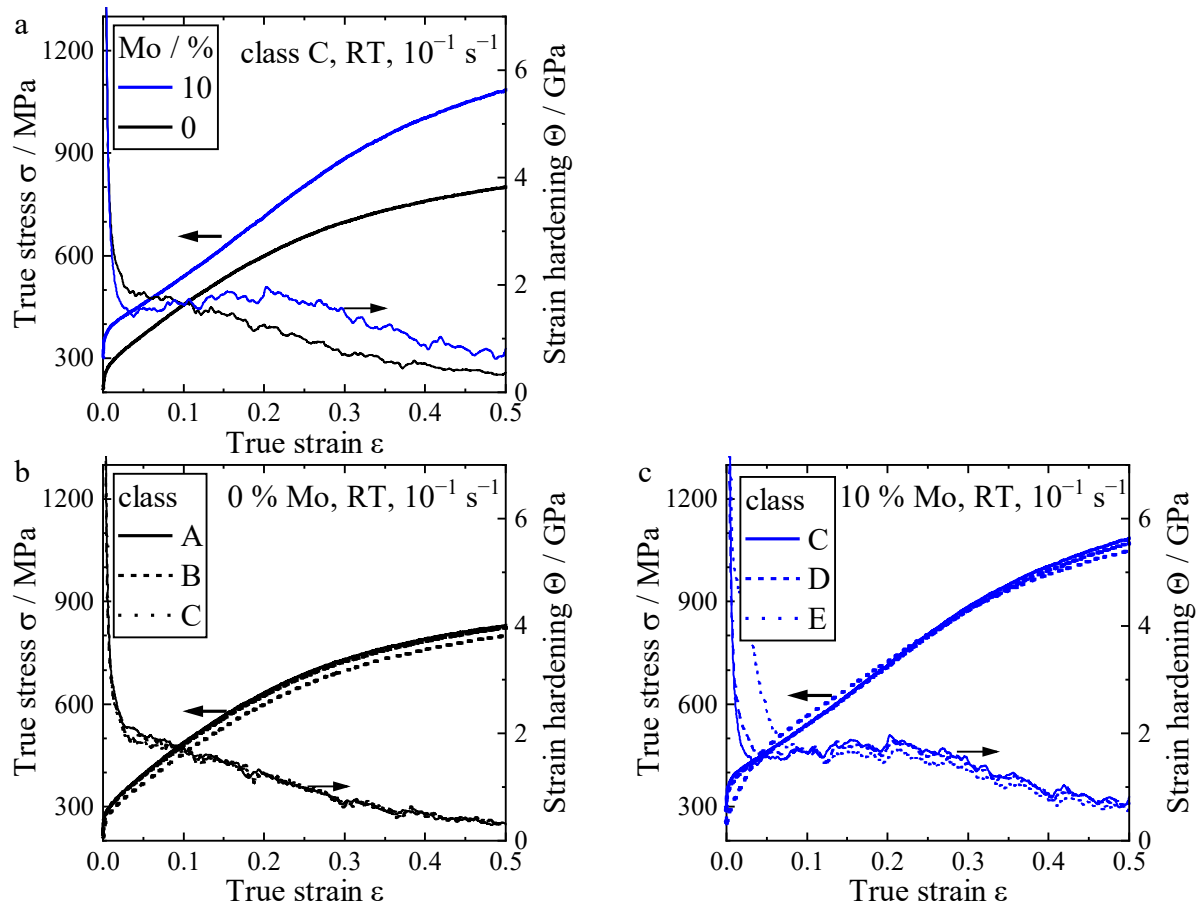

Fig. 2. True stress σ and strain hardening Θ as a function of true strain ε for (a) different Mo contents and (b+c) different grain sizes classes.

Effect of strain rate. Fig. 3 shows the strain rate dependence of the flow curves and the strain hardening coefficients. A positive strain rate effect was observed. Only at true strains below 0.1, there is practically no difference between the stresses at intermediate (10^2 s^{-1}) and high strain rates (10^3 s^{-1}) for the material with 0 % Mo. Independent of the Mo content, an increase in strain rate results in an increase in strain hardening. Furthermore, the sensitivity to an strain rate increase is higher in the materials without Mo. Starting at lower stress levels (cf. Fig. 2a), the stresses which were reached at the highest strain rate are similar to the stress levels of the material with 10 % Mo.

Even at the highest strain rate of 10^3 s^{-1}, the material with 0 % Mo shows no local maximum of the strain hardening coefficient, c.f. Fig. 3a. This local maximum was intensified for the material with 10 % Mo at higher strain rates. Furthermore, the maximum of the strain hardening coefficient was shifted to lower strains, c.f. Fig. 3b.
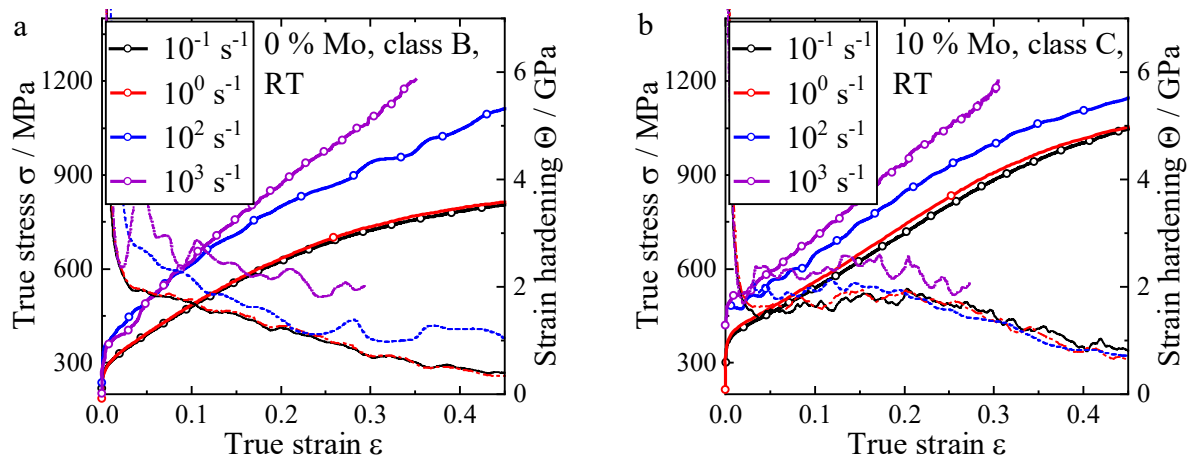
Fig. 3. True stress σ and strain hardening Θ as a function of true strain ε for different strain rates (a) with 0 % Mo and (b) 10 % Mo.

Effect of temperature. At a cryogenic temperature of −196°C the yield strength and strain hardening are higher than at ambient temperature, cf. Fig. 4a. The temperature effect on the flow stress at an intermediate strain rate of about 10^2 s^{-1} is more pronounced for the material with 10 % Mo addition, cf. Fig. 4b. The addition of 10 % Mo has a similar effect on the strain hardening as the decrease of temperature to −196°C. Like the tests at ambient temperature, the strain hardening behavior of the material with 10 % Mo is characterized by a local maximum, with highest strain hardening coefficient at −196°C.
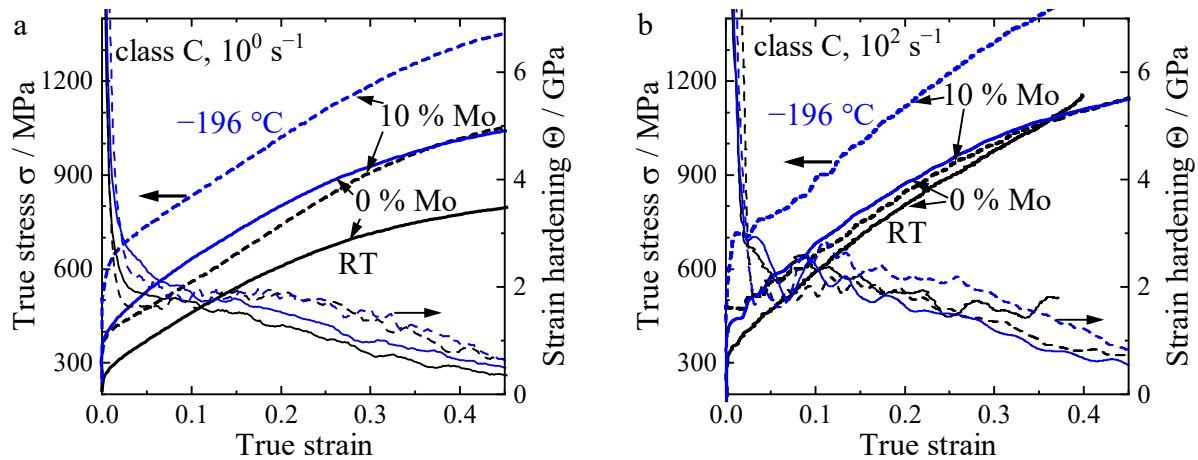

Fig. 4. True stress σ and strain hardening Θ as a function of true strain ε for different Mo contents and temperatures at strain rates (a) 10^{-1} s^{-1} and (b) 10^2 s^{-1}.

Microstructural development. To explain and discuss the mechanical behavior, the microstructure of selected tests was analyzed at different degrees of deformation. Firstly, interrupted compressive tests are discussed. Secondly, the microstructure at a true compressive strain of about 0.4–0.5 is evaluated.

From the EBSD measurements in Fig. 5 it was derived that the formation of twins is affected by temperature and strain rate. The basic relationships from other studies like [9] are also found here. At the highest strain rates in the present study, multiple twinning was observed even at relatively low strains of about 0.02. This phenomenon was not observed at tests below strain rates of 10^2 s^{-1}, even at cryogenic temperatures.
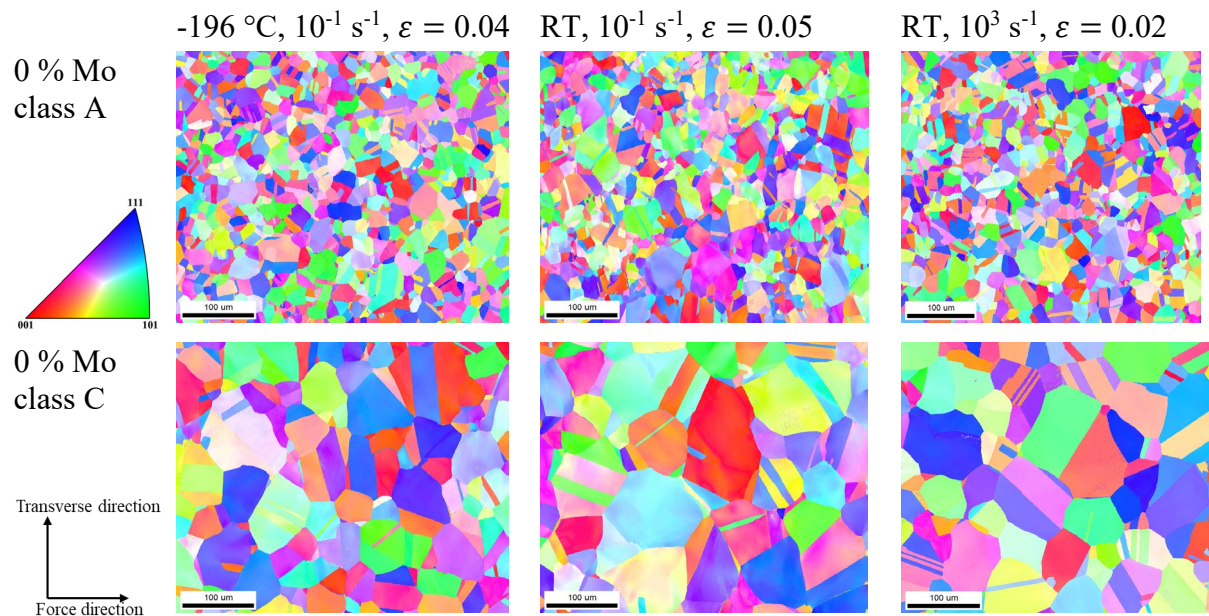
Fig. 5. Inverse pole figure visualizations of the microstructure after small deformation in materials with 0 % Mo: First row: smallest grain size, Second row: largest grain size. Effect of temperature from first to second column. Effect of strain rate from second to third column.

The EBSD results at large degrees of deformation are shown in Fig. 6. Due to the large deformation ($\varepsilon \approx 0.5$), the elongation of the grains is clearly visible. Moreover, there was further twinning within favorably oriented grains. A quantitative analysis of the $\Sigma 3$ grain boundaries, i.e. the twin planes, reveals a significantly higher amount of twinning after testing at cryogenic temperature. Furthermore, with the addition of 10 % Mo the effect of deformation twinning was already observable largely at room temperature and at relatively small strain rates.

The microstructural observations in Fig. 6 are well related to the mechanical behavior in Fig. 4. The material with 10 % Mo shows a relatively large strain hardening even at room temperature. To achieve a similar strain hardening for the materials without Mo, a temperature of -196 °C is needed. The pronounced effect of twinning formation leads to small free paths for dislocation motion and, hence, for high strength and high strain hardening.

The twins are already formed after a short amount of deformation, e.g. after reaching a threshold stress. Hence, the material with 10 % Mo exhibiting higher stress levels due to solid solution hardening shows a higher amount of strain hardening due to easier formation of twins. Similarly, lower temperatures and higher strain rates will increase the strain hardening in fcc materials, cf. Fig. 4. Hence, higher stress levels are reached after smaller deformation.
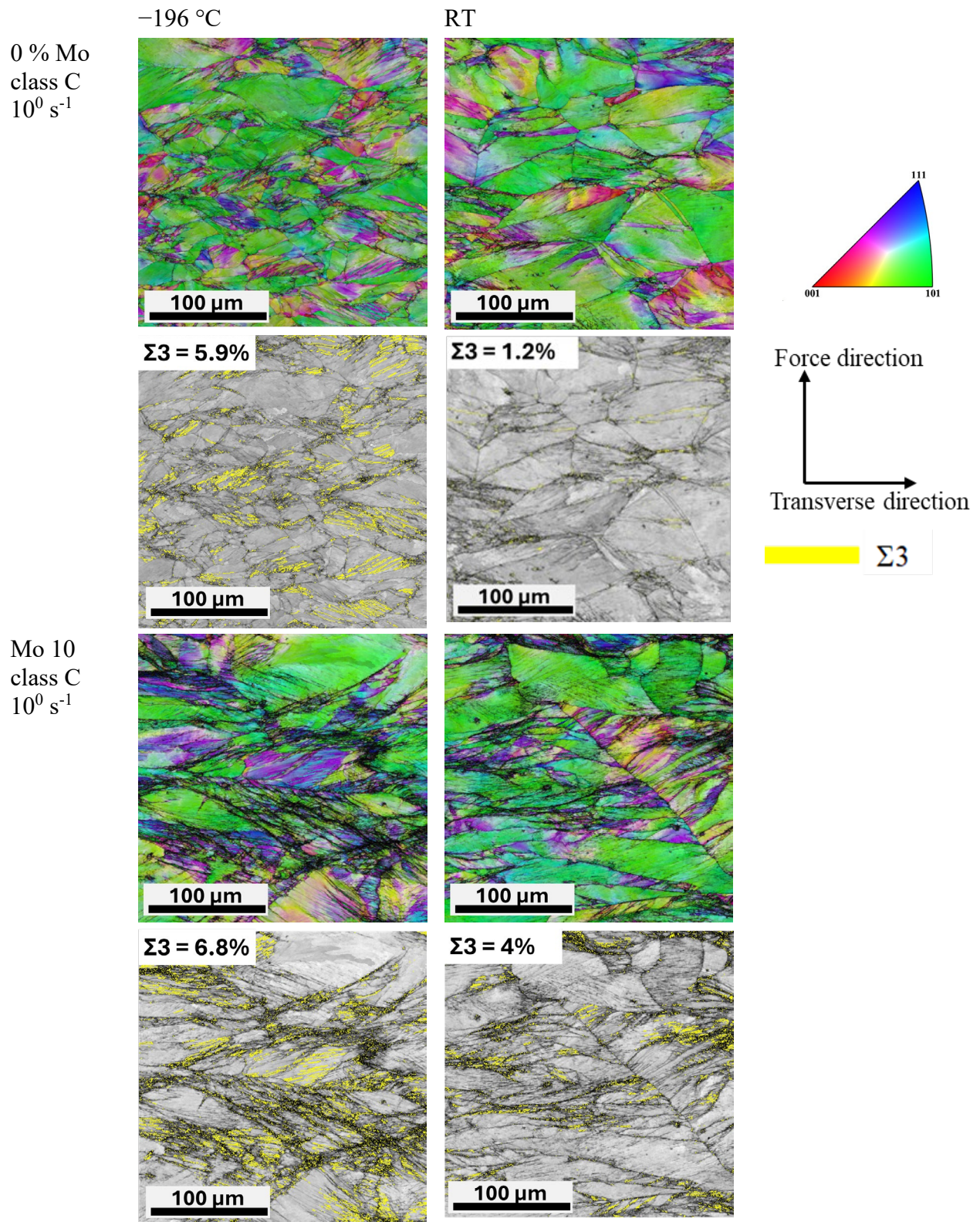
Fig. 6. Inverse pole figure visualization and image quality map with Σ3 grain boundary of the microstructure after deformation: Temperature effect from left to right column; Effect of Mo addition from upper to lower part of the figure.

Summary and Conclusions

The compressive loading behavior of high entropy alloys based on FeMnNiCo with and without Mo addition was investigated regarding grain size, strain rate, and temperature effects. To reveal the interdependencies between microstructure and mechanical properties, microstructural analysis of different deformation degrees was performed by means of SEM/EBSD. The following conclusions can be drawn:

- The addition of 10 % Mo significantly increases the susceptibility to form twins during deformation. This observation leads to higher strain hardening coefficients. Furthermore, the strain hardening shows a local maximum which is affected by temperature and strain rate.
- Higher strain rates and a cryogenic temperature result in higher stress levels and higher strain hardening. These observations are explained both by typical behavior of fcc metals and by pronounced twinning at lower temperatures and higher strain rates.
- Within the analyzed range, the mechanical behavior is relatively weakly affected by the grain size. Nevertheless, an decreased grain size will increase the flow stress.
- In all material conditions a damage tolerant compressibility without cracks on the surface of the samples was observed.

References

[1] B. Cantor, I. Chang, P. Knight, A. Vincent, Microstructural development in equiatomic multicomponent alloys, Mat. Sci. Eng. A 375-377 (2004) 213–218. https://doi.org/10.1016/j.msea.2003.10.257

[2] J.-W. Yeh, S.-K. Chen, S.-J. Lin, J.-Y. Gan, T.-S. Chin, T.-T. Shun, C.-H. Tsau, S.-Y. Chang, Nanostructured High-Entropy Alloys with Multiple Principal Elements: Novel Alloy Design Concepts and Outcomes, Adv. Eng. Mater. 6 (2004) 299–303. https://doi.org/10.1002/adem.200300567

[3] E.P. George, W.A. Curtin, C.C. Tasan, High entropy alloys: A focused review of mechanical properties and deformation mechanisms, Acta Mater. 188 (2020) 435–474. https://doi.org/10.1016/j.actamat.2019.12.015

[4] Z. Li, K.G. Pradeep, Y. Deng, D. Raabe, C.C. Tasan, Metastable high-entropy dual-phase alloys overcome the strength-ductility trade-off, Nature 534 (2016) 227–230. https://doi.org/10.1038/nature17981

[5] M.A. Meyers, O. Vöhringer, V.A. Lubarda, The onset of twinning in metals: a constitutive description, Acta Mater. 49 (2001) 4025–4039. https://doi.org/10.1016/S1359-6454(01)00300-7

[6] S. Basu, Z. Li, K. G. Pradeep, D. Raabe, Strain Rate Sensitivity of a TRIP-Assisted Dual-Phase High-Entropy Alloy, Front. Mater. 5 (2018). https://doi.org/10.3389/fmats.2018.00030

[7] A. Huang, S.J. Fensin, M.A. Meyers, Strain-rate effects and dynamic behavior of high entropy alloys, J. Mater. Res. Technol. 22 (2023) 307–347. https://doi.org/10.1016/j.jmrt.2022.11.057

[8] L.W. Meyer, N. Herzig, T. Halle, F. Hahn, L. Krüger, K.P. Staudhammer, A basic approach for strain rate dependent energy conversion including heat transfer effects: An experimental and numerical study, J. Mater. Process. Tech. 182 (2007) 319–326. https://doi.org/10.1016/j.jmatprotec.2006.07.040

[9] Z. Li, S. Zhao, R.O. Ritchie, M.A. Meyers, Mechanical properties of high-entropy alloys with emphasis on face-centered cubic alloys, Prog. Mater Sci. 102 (2019) 296–345. https://doi.org/10.1016/j.pmatsci.2018.12.003

[10] J.M. Park, J. Moon, J.W. Bae, M.J. Jang, J. Park, S. Lee, H.S. Kim, Strain rate effects of dynamic compressive deformation on mechanical properties and microstructure of CoCrFeMnNi high-entropy alloy, Mat. Sci. Eng. A 719 (2018) 155–163. https://doi.org/10.1016/j.msea.2018.02.031

[11] K. Cichocki, P. Bała, T. Kozieł, G. Cios, N. Schell, K. Muszka, Effect of Mo on Phase Stability and Properties in FeMnNiCo High-Entropy Alloys, Metall. Mater. Trans. A 53 (2022) 1749–1760. https://doi.org/10.1007/s11661-022-06629-x

[12] S. Henschel, L. Krüger, Dynamic crack initiation measurements in a four-point split Hopkinson bending device, Eng. Fract. Mech. 133 (2015) 62–75. https://doi.org/10.1016/j.engfracmech.2015.05.020